NASA/CR-1998-207628

NASA Contract Report

An Experimental Investigation of Transverse Tension Fatigue Characterization of IM6/3501-6 Composite Materials Using a Three-Point Bend Test

Ann W. Peck

University of Wyoming
Laramie, WY 82071-3295

Contract NAG1 - 1773

March 1998

NASA Contract Report

An Experimental Investigation of Transverse Tension Fatigue Characterization of IM6/3501-6 Composite Materials Using a Three-Point Bend Test

Ann W. Peck

University of Wyoming
Laramie, WY 82071-3295

Contract NAG1 - 1773

March 1998

PREFACE:

This final technical report presents the results of the efforts on NASA – Langley Research Grant NAG-1-1773. The NASA-Langley technical monitor was Dr. Raju Ivantury of the Mechanics of Materials Division.

The finite element analysis was performed by Dr. Ann Peck. The experimental tests (static and fatigue) were performed by the Composite Materials Research Group (CMRG) within the Department of Mechanical Engineering at the University of Wyoming. Mr. Scott L. Coguill and Ms. Ronda Coguill were the major contributors to this effort. Compilation and analysis of the experimental results were performed by Dr. Peck.

Use of commercial products or names of manufacturers in this report does not constitute official endorsement of such products or manufacturers, either expressed or implied, by the National Aeronautics and Space Administration.

TABLE OF CONTENTS

LIST OF FIGURES

LIST OF TABLES

ABSTRACT: As composites are introduced into more complex structures with out-of-plane loadings, a better understanding is needed of the out-of-plane, matrix-dominated failure mechanisms. This work investigates the transverse tension fatigue characteristics of IM6/3501 composite materials. To test the 90 degree laminae, a three-point bend test was chosen, potentially minimizing handling and gripping issues associated with tension tests. A finite element analysis was performed of a particular specimen configuration to investigate the influence of specimen size on the stress distribution for a three-point bend test. Static testing of 50 specimens of 9 different sized configurations produced a mean transverse tensile strength of 61.3 Mpa (8.0 ksi). The smallest configuration (10.2 mm wide, Span-to-thickness ratio of 3) consistently exhibited transverse tensile failures. A volume scale effect was difficult to discern due to the large scatter of the data. Static testing of 10 different specimens taken from a second panel produced a mean transverse tensile strength of 82.7 Mpa (12.0 ksi). Weibull parameterization of the data was possible, but due to variability in raw material and/or manufacturing, more replicates are needed for greater confidence. Three-point flex fatigue testing of the smallest configuration was performed on 59 specimens at various levels of the mean static transverse tensile strength using an R ratio of 0.1 and a frequency of 20 Hz. A great deal of scatter was seen in the data. The majority of specimens failed near the center loading roller. To determine whether the scatter in the fatigue data is due to variability in raw material and/or the manufacturing process, additional testing should be performed on panels manufactured from different sources.

KEYWORDS: composite materials, graphite/epoxy, transverse tensile strength, flexural fatigue, Weibull statistics

INTRODUCTION

A great deal of research has been performed characterizing the in-plane fiber-dominated properties, under both static and fatigue loading, of advanced composites materials. This understanding is imperative wherever composite materials are used in order to gain a better understanding of the reliability of structures when designing for maximum efficiency in weight, volume, and payload. However, as composites are introduced into more complex loading states, there is a need to better understand some of the out-of-plane and matrix-dominated phenomena which have not received as much attention. For instance, consider the design of bonded composite airframe structure where repeated, cyclic out-of-plane bending may occur. Two such scenarios where this loading may take place are in a compressively loaded post-buckled panel or a full-scale pressurized fuselage such as the one investigated by the NASA Advanced Composite Technology (ACT) program. In the latter case, as a result of the internal pressurization within each panel bay, the skin will bulge or "pillow" as shown in Figure 1. These out-of-plane deformations create local bending moments along the skin-stiffener and skin-frame interfaces, which in turn create shear and peel stresses along the various bondline [*1*].

Recent tests characterizing skin/stringer debond failures in reinforced composite panels where the dominant loading in the skin is flexure along the edge of the frame indicate failure initiates as transverse matrix cracks either in the skin or the flange near the flange tip [*2*]. When failure initiated in the skin, transverse matrix cracks formed in the surface ply closest to the flange and either initiated delaminations or created matrix cracks in the next lower ply, which in turn initiated delaminations. When failure initiated in the flanges, transverse cracks formed in the flange angle ply closest to the skin and initiated delaminations. In no configuration did failure propagate through the adhesive bond layer. This is a significant finding in that the limiting

component in this particular bonded structure under internal pressurization appears not to be the adhesive, but rather the particular skin and flange laminates, and in particular the choice and location of the angle plies. The failure initiation site corresponded well with the site of maximum transverse tension stress, not the site of maximum interlaminar tension site. For the examined skin/flange configuration, the maximum transverse tension stress at failure correlated well with the transverse tension strength of the composite [*2*]. Therefore, it is important to understand how the transverse strength of the composite degrades under repeated cyclic loading.

An extensive literature search on the topic of transverse tension fatigue revealed little in the published literature on this particular topic. Perhaps this is a result of the focus, to-date, on in-plane loaded structures, such as composite wing skins, where matrix cracking in fatigue may be a rare occurrence at the relatively low operating strains dictated by low velocity impact concerns, and where matrix cracks are fairly benign if they do occur. However, for the out-of-plane loads experienced in a composite fuselage, the onset of matrix cracking under repeated pressurization may trigger a catastrophic failure. Hence, the need for a transverse tension fatigue characterization is now apparent. It should be noted that there has been extensive work, both theoretical and experimental, focusing on transverse crack formation in laminates under fatigue loading [3]. The laminates studied have generally consisted of 90 degree plies embedded within a general composite laminate which usually also included 0 degree and ±45 degree plies. The crack formation and corresponding failure stress in the 90 degree plies of the laminates differs substantially due to the constraining effect of the non-90 degree plies. This study will focus on the failure behavior of unconstrained 90 degree plies.

When testing 90 degree laminae, several issues must be addressed. The first is the concern over handling and gripping sensitivities. The handling and gripping issues may be minimized by

testing in three-point bending as opposed to testing in tension. This has an additional benefit in that relatively small specimen sizes may be used, thereby reducing the amount of material needed for a single replicate. A small specimen size has the added benefit of minimizing internal heating due to the cyclic loading, and hence, allowing higher frequencies, with shorter testing times, to be performed. This can become significant for a test that potentially may become a standard for fatigue characterization. Adams, King, and Blackketter [*4*] evaluated the transverse flexure test using unsized AU4 and AS4 fibers, sized AS4 fibers and EPON 828 resin. Span-to-thickness ratios of the specimens ranged from 4.0 to 16.7. All the specimens produced tensile failures and yielded similar strengths. The transverse flexure tests produced higher values of the transverse tensile strength than standard transverse tensile tests, by as great as a factor of 2.5, as demonstrated by the AS4/EPON 828 combination.

The transverse tension strength of graphite epoxy composites has been shown to exhibit a volume dependence due to the inherent flaws in the microstructure. O'Brien and Salkepar investigated the volume scale effect using AS4/3501-6 90° tensile specimens [*5*]. They found the transverse tensile strength of composite laminate depends on the volume of material stressed. The dependence reflects the presence of inherent flaws in lamina's microstructure. As the volume of material under tension increases, transverse tensile strength decreases. The probability distribution function of the strength as defined by Weibull [*6*] is

$$P(\sigma) = 1\text{-}exp^{-}(\sigma/\sigma_c)^m \tag{1}$$

where m is the shape parameter, indicating the measure of scatter in the data, and σ_c is the location parameter, similar to the mean of a normal distribution. Specimens of different volumes

$$\frac{(\sigma_{ult})_1}{(\sigma_{ult})_2} = -\left(\frac{V_2}{V_1}\right)^{1/m} \tag{2}$$

can then be compared via a Weibull scaling law for static loading which states

where $(\sigma_{ult})_1$ and $(\sigma_{ult})_2$ are the different strengths associated with the different specimens volumes V_1 and V_2 and m is a material constant found experimentally.

The primary objective of this study was to experimentally investigate the transverse strength of a composite under repeated cyclic loading. In this study, multiple 90° laminates of different specimen sizes were tested in flexure under static loading to first determine an optimum specimen configuration with 'optimum' being defined as the smallest sized configuration producing transverse tensile failures consistently. Using the optimum sized configuration, multiple 90° laminates were tested in flexure under cyclic loading to first investigate the behavior of transverse tensile strength under fatigue loading. The data was then used to evaluate the validity of the Weibull scale law for fatigue loading. Additional tests were conducted at different frequencies to determine if the transverse tension fatigue strength exhibits a frequency dependency.

FINITE ELEMENT ANALYSIS

Model Definition

A nonlinear static finite element analysis was performed using the pre-processing software package PATRAN and its P3/FEA solver package. Figure 2 provides a schematic of the test set-up with relevant dimensions while Figure 3 shows the experimental three-point bend test set-up. A 2-D model was constructed. Due to symmetry considerations, only the right half of the specimen was modelled. Figure 4 shows the finite element mesh of the model. The mesh contained 1680 4-noded quadrilateral elements and 21 gap elements for a total of 3622 degrees of freedom. The specimen geometry itself is very straight forward: half of the rectangular test specimen. The loading and support rollers were modelled as follows. Only the lower right hand exterior edge of the central 0.25 inch diameter loading roller surface was modelled. Eleven nodes were placed along the arc representing the lower righthand edge of the roller. Gap elements, which are the source of the analysis'nonlinearity, connected this surface to the upper left hand section of the finite element model, which corresponds to the midsection of the upper surface of the actual test specimen. The upper lefthand quarter of the 0.125 inch diameter support roller was modelled as a block of 0.0625 inch width and depth with the isotropic properties of steel (E = 29.0 Msi, ν = 0.3). Gap elements connected the lower right hand section of the specimen to the loading block. The gap lengths corresponded to the vertical distances between the lower righthand section of the specimen and the upper lefthand surface of a 0.125 inch diameter roller. The gap stiffnesses were determined by varying the stiffnesses, running the model, and observing the final deformations of the rollers and laminate. This variation was

performed until reasonable deformation results were obtained. A single point load representing the average static failure load was applied at the bottom of the loading block.

Three different material systems were defined:

Isotropic steel:	E = 29.0 Msi, $\nu = 0.3$
Isotropic 90 degree IM6/3501-6 tape:	E = 1.4 Msi, $\nu = 0.45$
Orthotropic IM6/3501-6 composite:	E11=21.0 Msi, E22 = E33 = 1.4 Msi, $\nu_{12} = \nu_{13} = 0.3$, $\nu_{23} = 0.3$ G12 = G13 = 0.75 Msi, G23 = 0.50Msi

The lower loading block mesh consisted of 80 4-noded quadrilateral elements subject to the plane strain condition and assigned the material properties of steel. The main laminate consisted of 1600 4-noded quadrilateral elements. The laminate was modelled under both plane stress and plane strain conditions. The laminate was modelled first with isotropic 90 degree IM6/3501-6 tape properties and then with orthotropic IM6/3501-6 composite properties.

Model Results

The first portion of the finite element analysis focused on examining the smallest sized specimen configuration (w = 0.400 inches, t= 0.266 inches, $(S/t) = 3$) under several different conditions. In each case, an applied loading corresponded to 114.5 lb was assigned to the lower right node of the steel (plane strain) loading block. The specimen itself was modelled with the following conditions:

	Laminate Element Properties	Laminate Material Properties
Case 1:	Plane Strain	Isotropic 90 degree IM6/3501-6 tape
Case 2:	Plane Stress	Isotropic 90 degree IM6/3501-6 tape
Case 3:	Plane Stress	Orthotropic 90 degree IM6/3501-6 composite

There was little differences in the laminate local stresses (σ_x, σ_y, τ_{xy}) for the three different cases. The local stresses were defined with *x* along the horizontal of the specimen and *y* along the vertical of the specimen. A positive shear stress exists when positive *x*, positive *y* corner of a 2-D element the element wants to move in the positive *x* and negative *y* directions. Table 1 compares the different local stresses for several elements for the three cases described above. Figure 5 shows the location of the different elements on the mesh. Figures 6 through 8 show the contour plots of the different stresses.

TABLE 1-- Comparison of Longitudinal, Transverse, Shear Stresses from Finite Element Analyses

	Global Longitudinal Stresses, σ_x (Psi)			Global Transverse Stresses, σ_y (Psi)			Global Shear Stresses, τ_{xy} (Psi)		
Element ID	Isotropic Plane ε	Isotropic Plane σ	Orthotropic Plane σ	Isotropic Plane ε	Isotropic Plane σ	Orthotropic Plane σ	Isotropic Plane ε	Isotropic Plane σ	Orthotropic Plane σ
4290	8743	8803	8760	2.5	1.01	0.9	3	3	3
4300	6117	6161	6159	-177	-177	-173	57	57	56
4400	1642	1652	1663	-1329	-1391	-1371	145	145	143
4439	-440	-442	-445	-250	-247	-256	1656	1656	1661
4500	-3243	-3280	-3279	-5531	-5522	-5461	622	613	607
4590	-27900	-27430	-27500	-30060	-28750	-28770	12430	12720	12850
4599	-5750	-5814	5805	6.6	2.6	2.5	41	38	38

The next section will focus on the results of the orthotropic plane stress model. At the centerline of the specimen, the maximum longitudinal tensile stress on the lower surface (element 4290, σ_x = 8760 psi) is substantially lower than the maximum longitudinal compressive stress on the upper surface of the specimen (element 4590, σ_x = -27500 psi). However,

examining the compressive stresses in the elements just below the upper surface, the magnitude of the compressive stresses (element 4570, σ_x = -9846 psi, element 4560, σ_x = -7638 psi) are approximately the same as those of the tensile stresses near the lower surface. The discrepancy is due to the immediate contact of the specimen with the upper roller support and the minimal discretization of the finite element mesh at this particular loading location.

The maximum shear stress was located off the centerline of the specimen and approximately at the midplane of the specimen's thicknesses. The maximum shear stress of the orthotropic plane stress case was approximately 1600 psi.

Again considering the orthotropic plane stress case, at the centerline of the specimen, the maximum transverse stress is located on the upper surface of the specimen at its centerline (element 4590, σ_y = -28770 psi). Moving down through the specimen thickness along the centerline, the local transverse stresses decline. At the lower surface of the specimen, the transverse stress is negligible (element 4290, σ_y = 0.9 psi). Considering the transverse stresses of the elements located approximately 10% of the half-specimen length off the specimen centerline and moving down through the specimen thickness, the magnitudes decrease from –2400 psi (element 4503, located approximately 20% of the thickness from the upper surface) to –1100 psi (element 4403, located approximately 50% of the thickness from the upper surface) to –25 psi (element 4253, located approximately 7% of the thickness from the lower surface).

From a "Strength of Materials" approach, the ratio of maximum transverse stress to maximum shear stress for the three-point bend test equals twice the span-to-thickness (S/t) ratio [*2*]. The maximum transverse stress would appear at the outer surfaces of the specimen's center location with respect to length. The shear stress distribution would be a parabolic distribution through the thickness with the maximum stress appearing at the midplane of the specimen's thickness. The

finite element analysis predicted the maximum tensile stress on the lower surface of the specimen's centerline (element 4290, σ_x = 8760 psi) and the maximum shear stress approximately at the midplane of the specimen's thickness (element 4439, 1660 psi). For the modelled specimen configuration (w = 0.400 inches, t = 0.266 inches , (S/t) = 3), the maximum transverse stress to maximum shear stress ratio should equal 6. Comparing the above stated stresses, the finite element model predicted the ratio of transverse stress to maximum shear stress to be a value of 5.28.

The different strengths associated with unidirectional AS/3501 graphite/epoxy composites [7], similar to the IM6/3501-6 material system which was used in the finite element model, are listed below.

Longitudinal Properties:	σ_{LT} ~210 Ksi (1447 Mpa)	σ_{LC} ~210 Ksi (1447 Mpa)
Transverse Properties:	σ_{TT} ~ 7.5 Ksi (51.7 Mpa)	σ_{TC} ~ 29.9 Ksi (206 Mpa)
Shear Properties:	τ_{12} ~ 13.5 Ksi (93 Mpa)	

Comparing the different stresses induced in the specimen under a 114.5 lb force, the specimen's maximum longitudinal stress of 8760 psi corresponds closely to the transverse tensile strength. The longitudinal compressive stresses near the center roller approach the transverse compressive strength. However, further refinement of the model, namely further discretization of the mesh, near the support would be necessary to validate if those stresses are accurate or erroneous due to a coarse model near a reaction point.

MATERIALS AND SPECIMEN PREPARATION

Two 30.48 cm by 45.72 cm (12 inch by 18 inch) panels of unidirectional prepreg IM6/3501-6 graphite/epoxy material were layed up and cured in an autoclave according to the manufacturer's specifications. The nominal cured ply thickness is 0.188 mm (0.0074 inch). Each panel was constructed of 36 plies.

The two panels were ultrasonically C-scanned after manufacturing to assess the integrity of the manufacturing process. Each panel exhibited patches of possible voids, located near the borders of the panels. The first panel exhibited a greater amount of non-uniformity than the second panel. Using the C-scans as a guide, specimens were cut from the regions of the panels exhibiting the most uniform C-scan patterns.

Nine different test specimen configurations were used in the static study. Table 2 indicates the different widths (w) and span-to-thickness (S/t) ratios examined. Different sized configurations were tested as an initial objective of this study was to determine the minimum-sized specimen configuration which would consistently generate a transverse tensile failure under three-point bending.

TABLE 2-- Static Test Specimen Configurations and Number of Test Samples.

Specimen Configurations and Number Tested				
Nominal Width, w (mm) [a]	Span-to-thickness Ratio, (S/t) [b,c]			
	3	4	6	8
10.2 (0.40)	A (7)	D (10)	G (2)	K (3)
12.7 (0.50)	B (10)	E (9)	...	...
15.2 (0.60)	C (6)	F (10)	...	M (3)

[a] Number in parentheses is value in inches where 1 in. = 25.4 mm
[b] Letter indicates Specimen Configuration
[c] Number in parentheses is number of samples tested

The first set of static specimens was cut from Panel #1 using a diamond-wheel saw blade. Edges were not polished before testing so as not to bias results by reducing edge flaws or possibly internal flaws. Static and fatigue specimens from Panel #2 were cut using a water-cooled aluminum oxide abrasive wheel (180 grit) then edge ground to their final dimensions. Specimen sizes were determined per a pre-established cutting plan, which purposely distributed the different configuration sizes throughout the panel so as not to concentrate a single configuration to one area of the panel. The specimen cross-sectional dimensions were measured using ball-point calipers at the center location along the specimen length. A single length measurement was taken along the centerline of the specimen.

Table 3 shows the average nominal ply thicknesses of the static and fatigue specimens. The average laminate thickness for the specimens tested from a particular panel and under a particular loading (static vs fatigue) was divided by the number of plies to obtain a nominal ply thickness (t). The product of the nominal ply thickness and the manufacturer's supplied fiber density (1.7325 g/cm^3) was divided into the assumed fiber aerial weight (190 g/m^2) for IM6/3501-6 to obtain estimated fiber volume fractions. These estimated fiber volume fractions are compared with experimentally measured fiber volume fractions in Table 3.

TABLE 3--Nominal Ply Thickness and Fiber Volume Fractions, IM6/3501-6 graphite-epoxy.

	Panel #1		Panel #2			
	Static [a,b]		Static [a,b]		Fatigue [a,b]	
Nominal Ply Thickness, t (mm)	0.188 (0.0074)	[0.99]	0.191 (0.0075)	[1.0]	0.191 (.0075)	[1.02]
Estimated V_f, %	58.0	...	57.9	...	57.7	...
Measured V_f, %	59.4	[0.84]	59.8	[1.31]	...	...

[a] Number in parentheses is value in inches where 1 in. = 25.4 mm
[b] Number in brackets is Coefficient of Variation

Visual examination of the specimens revealed pitting in the majority of the fatigue specimens. In most instances, the pits were approximately pinpoint in size and shallow in depth. In a few instances, the pits were larger in size. The pits were located within approximately the upper 25% of the laminate thickness as measured from the upper surface of the specimen, which corresponds to the bottom surface of the manufactured panel. The number of pinpoint-sized pits in a particular specimen was of the order of 20 to 30. The pits were distributed along the length of the specimens. Because the pits were located on the compressive side of specimens when loaded, they were not believed to have a significant effect on the results.

EXPERIMENTAL PROCEDURE

Fiber volume measurements were performed per the following ASTM standards: *D3171 Fiber Volume by Acid Digestion, D792 Density by Water Displacement*, and *D2734 Void Content.*

Static transverse tension tests were performed using the three-point flex procedure as specified in *ASTM D790-92, Standard Test Method for Flexural Properties of Unreinforced and Reinforced Plastics and Electrical insulating Materials.* Figure 2 provides a schematic of the test set-up with relevant dimensions. The fixture was equipped with 6.35 mm (0.25 inch) diameter loading roller and 3.175 mm (0.125 inch) diameter support rollers. Span-to-thickness (S/t) ratios of 3, 4, 6, and 8 were used as required for the static tests. The support rollers were located using the center loading roller as a datum. The specimens were loaded into the fixture with the midpoint of the specimen aligned under the loading roller. Adjustments to the centering of the specimen were made by eye. As the specimens were fairly short in length, there was little extension of an individual specimen beyond the support rollers. All specimens were tested with the compression face of the specimen corresponding to the bottom of the panel. The fixture was mounted on a 22.24 kN (5000 lb) MTS brand servo-hydraulic universal test frame with an MTS TestStar digital controller under ambient laboratory conditions, as shown in Figure 3. The test frame has a current certification of calibration providing traceablility to NIST standards. Static tests were performed at a constant ram speed of 1.27 mm/min (0.05 in/min) with a stroke range set at 12.7 mm (0.5 inches). After an individual specimen failure, the specimen was removed and the moment arm distance from the centerline of the edge support roller to the location of tensile failure, defined as l, measured. The bending moment was calculated as the product of

half the failure load P and the moment arm (l). The nominal transverse tensile stress was calculated as

$$\sigma = \frac{(\frac{1}{2}P)l}{(\frac{1}{12})wt^3} \tag{3}$$

using the nominal cross-sectional dimensions w and t. Local cross-sectional dimensions were taken close to the failure location.

Fatigue tests were performed at a variety of frequencies and amplitudes under load control. The specimens were mounted in the same machine under the same procedure as described above for the static specimens. Fatigue tests were performed at a constant ram speed of speed of 1.27 mm/min (0.05 in/min) with a stroke range set at 12.7 mm (0.5 inches). The average ultimate transverse tensile strength (UTS) obtained from the Panel #2 "A" configuration static specimens (w = 10.2 mm and (S/t) = 3) was used to calculate the load levels for fatigue. The majority of fatigue tests were run under the conditions R = 0.1, where R equals the ratio of the minimum applied load to the maximum applied load. Tension-tension fatigue tests were performed at 75%, 80%, 85%, 95% UTS levels with a frequency of ω equal to 5 Hz. Additional tests were performed at ω equal 20 Hz to examine the effect of frequency. A few tests were run at R = 0.5 to examine the effect of load ratio. Tests were stopped at 10^5 cycles if no failure occurred. Several tests were run beyond that limit and stopped at 10^6 cycles if no failure occurred. The same operator conducted all the fatigue tests.

EXPERIMENTAL RESULTS

Material Properties of Fiber Volume

The fiber, resin, and void volume fractions were determined according to ASTM specifications assuming a resin density of 1.262 g/cm^3 and fiber density of 1.7325 g/cm^3. Tests were performed on three specimens from each of the two panels. The measured fiber volume values are given in Table 3 with the coefficient of variation values shown in brackets. The estimated fiber volume fractions are slightly lower than the measured values. The high variability in laminate thickness contributes to the deviation in the estimated and measured fiber volume fraction values.

Transverse Tensile Static Strength Measurements

A summary of the results of the static tests is seen in Table 4. Individual specimen data (static loading) are found in Table 5. The nominal strengths are listed for the different configurations using the nominal cross-sectional dimensions of the individual specimens. Strengths are also listed for the different configurations using the local cross-sectional dimensions measured as described in the Experimental Procedure section. The coefficients of variation of the strength for the different configurations are also given. The number of specimens tested per configuration is given in Table 2 (see page 10).

All the specimens exhibited a transverse tensile failure regardless of the width or span-to-thickness ratio. For the specimens of (S/t) equal 3, the nominal transverse tensile strength increased as the width increased. For the specimens of nominal width 10.2 mm (0.4 in), there was little difference in strength except when (S/t) equaled 6. Only two specimens of that particular configuration were tested. The coefficient of variations (CV) for the different

configurations ranged from 7.8, corresponding to Configuration G ((S/t) = 6, W = 10.2 mm) to 33% for Configuration C ((S/t) = 3, W = 15.2 mm). The average CV for the nominal transverse tensile strength for Panel #1 was 22.1%. Because of the large scatter in strength of the different sized specimens from Panel #1, specimens for the smaller configurations (A & B) were tested from the second panel. The overall nominal transverse tensile strength was considerably higher (87.5 MPa) in Panel #2 compared to Panel #1 (61.3 MPa). Five specimens of configuration A and B were each tested. The CV's were considerably smaller with an overall average CV of 8.0% for Panel #2 static transverse tensile strength.

Figures 9 and 10 show the static strengths for the various specimens from Panel #1 as a function of the nominal cross-sectional area and the ratio of (S/t). Each plot shows a great deal of scatter for a given width or (S/t) ratio. Assuming a volume dependency on the strength, the strength should decrease with increasing cross-sectional area for a given width. This trend is not

TABLE 4--Summary of Nominal and Local Transverse Tensile Strength in MPa for 90° bend tests, IM6/3501-6 graphite-epoxy.

	Nominal Transverse Tensile Strength				
	Panel #1				Panel #2
	(*S/t*)				(*S/t*)
Width, *w* (mm)	3	4	6	8	3
10.2	56.3 [15.9]	59.6 [13.7]	68.9 [15.7]	59.5 [9.98]	91.7 [8.9]
12.7	58.5 [15.6]	63.1 [18.8]	...	...	82.7 [7.1]
15.2	67.5 [23.6]	67.5 [14.3]	...	52.4 [6.58]	...

	Local Transverse Tensile Strength				
	Panel #1				Panel #2
	(*S/t*)				(*S/t*)
Width, *w* (mm)	3	4	6	8	3
10.2	57.7 [13.3]	60.3 [31.5]	69.6 [8.35]	60.2 [9.95]	91.0 [8.8]
12.7	59.1 [15.9]	63.7 [28.6]	...	...	82.0 [6.8]
15.2	67.9 [33.1]	68.2 [13.6]	...	52.9 [12.6]	...

[a] Number in brackets is Coefficient of Variation

TABLE 5--Individual Specimen Data for Transverse Tensile Strength, 90° Bend Tests.

Specimen ID	(S/t)	Nominal Width, w (mm)	Nominal Thickness, t (mm)	Local Width, w (mm)	Local Thickness, t (mm)	Failure Load, P (N)	Moment Arm, l (mm)	Nominal Stress, σ (MPa)	Nominal CV (%)	Local Stress, σ (MPa)	Local CV (%)
PANEL 1 RESULTS											
SA4	3	10.26	6.83	10.24	6.82	1108	9.19	63.8		64.2	
SA5	3	10.26	6.76	10.27	6.75	894	11.73	67.2		67.2	
SA7	3	10.26	6.93	10.26	6.47	925	7.33	41.2		47.4	
SA8	3	10.29	6.91	10.26	6.89	970	9.73	57.6		58.1	
SA9	3	10.29	6.78	10.26	6.77	943	8.36	50.0		50.2	
SA10	3	10.31	6.73	10.26	6.71	974	9.31	58.2		58.9	
						969		**58.3**	**15.9**	**57.7**	**13.4**
SB1	3	12.47	6.83	...	...	1259	10.54	68.4		...	
SB2	3	12.47	6.78	...	...	1232	6.99	45.0		...	
SB3	3	12.80	6.88	...	...	1303	9.31	60.0		...	
SB4	3	12.78	6.83	12.78	6.82	1210	8.07	49.1		49.3	
SB5	3	12.80	6.76	12.78	6.73	1139	9.65	56.4		57.0	
SB6	3	12.80	6.76	12.83	6.76	1343	9.22	63.6		63.5	
SB7	3	12.80	6.93	12.80	6.91	1183	10.98	63.3		63.8	
SB8	3	12.80	6.88	12.80	6.88	1214	11.96	71.8		71.9	
SB9	3	12.80	6.78	12.80	6.76	1299	9.56	63.3		63.7	
SB10	3	12.80	6.91	12.78	6.89	1112	8.14	44.4		44.8	
						1229		**58.6**	**15.6**	**59.1**	**15.9**
SC1	3	15.19	6.81	15.19	6.80	1730	12.90	95.1		95.2	
SC2	3	15.21	6.78	15.18	6.79	1512	6.03	39.1		39.1	
SC3	3	15.34	6.88	15.34	6.87	1481	10.02	61.3		61.4	
SC4	3	15.16	6.86	15.14	6.82	1290	10.41	56.5		57.1	
SC5	3	15.14	6.73	15.16	6.72	1174	11.61	59.6		59.7	
SC6	3	15.34	6.86	15.29	6.84	1801	12.53	93.9		94.8	
						1498		**67.6**	**23.6**	**67.9**	**33.1**
SD1	4	10.13	6.78	...	...	752	12.24	59.2		...	
SD2	4	10.13	6.81	...	...	841	12.07	64.8		...	
SD3	4	10.13	6.78	...	...	863	9.44	52.4		...	
SD4	4	10.29	6.83	10.21	6.82	743	14.73	68.4		69.0	
SD5	4	10.21	6.93	10.19	6.92	974	13.69	81.5		82.1	
SD6	4	10.21	6.83	10.20	6.85	721	12.44	56.4		56.1	
SD7	4	10.21	6.73	10.20	6.72	707	9.94	45.6		45.7	
SD8	4	10.21	6.73	10.21	6.71	934	14.14	85.7		86.2	
SD9	4	10.26	6.76	10.20	6.76	543	12.19	42.4		42.6	
SD10	4	10.24	6.81	10.21	6.79	538	11.73	39.9		40.3	
						761		**59.6**	**13.7**	**60.3**	**31.5**
SE1	4	12.93	6.78	12.88	6.75	596	11.58	34.8		35.3	
SE3	4	12.93	6.81	12.90	6.78	1094	13.92	76.3		77.0	
SE4	4	12.80	6.86	12.80	6.83	1063	17.41	92.2		93.0	
SE5	4	12.75	6.93	12.72	6.91	850	14.38	59.8		60.4	
SE6	4	12.73	6.86	12.73	6.84	987	10.11	50.0		50.3	
SE7	4	12.75	6.73	12.76	6.69	752	11.28	44.0		44.5	
SE8	4	12.78	6.73	12.73	6.70	898	13.39	62.3		63.1	
SE9	4	12.78	6.76	12.75	6.75	1014	13.97	72.9		73.1	
SE10	4	12.75	6.81	12.76	6.80	850	17.68	76.3		76.4	
						900		**63.2**	**18.8**	**63.7**	**28.6**
SF1	4	15.29	6.81	15.29	6.77	1050	13.09	58.2		58.8	
SF2	4	15.32	6.81	15.32	6.79	1317	14.96	83.3		83.7	
SF3	4	15.32	6.78	15.34	6.78	1339	10.29	58.7		58.6	
SF4	4	15.34	6.73	15.32	6.72	1054	14.58	66.4		66.7	
SF5	4	15.19	6.96	15.18	6.91	1156	15.01	70.8		71.9	
SF6	4	15.16	6.83	15.16	6.81	885	14.58	54.7		55.0	
SF7	4	15.19	6.73	15.14	6.71	1245	12.01	65.2		65.9	
SF8	4	15.16	6.73	15.13	6.67	1183	15.30	79.0		80.6	
SF9	4	15.16	6.78	15.14	6.75	947	17.20	70.1		70.9	
SF10	4	15.16	6.81	15.13	6.79	987	16.51	69.6		70.0	
						1116		**67.6**	**14.3**	**68.2**	**13.6**
SG1	6	10.11	6.93	10.08	6.90	480	24.56	72.8		73.7	
SG2	6	10.11	6.73	10.08	6.73	507	19.65	65.3		65.5	
						494		**69.0**	**15.7**	**69.6**	**8.35**
SK1	8	10.29	6.88	10.29	6.86	356	30.05	65.8		66.3	
SK2	8	10.29	6.71	10.25	6.67	329	25.07	53.5		54.3	
SK3	8	10.29	6.76	10.25	6.74	311	29.88	59.4		60.0	
						332		**59.6**	**10.0**	**60.2**	**9.95**
SM1	8	15.19	6.91	15.19	6.87	567	22.92	55.7		56.4	
SM2	8	15.24	6.71	15.19	6.68	498	25.98	56.7		57.3	
SM3	8	15.21	6.76	15.19	6.74	409	25.40	44.9		45.3	
						498		**52.4**	**6.58**	**53.0**	**12.6**
PANEL 2 RESULTS											
PSA11	3	10.21	6.71	10.21	6.76	1379	9.98	89.9		88.6	
PSA12	3	10.19	6.83	10.21	6.83	1339	9.83	83.0		82.8	
PSA13	3	10.26	6.86	10.21	6.91	1659	9.93	102.4		101.4	
PSA14	3	10.24	6.86	10.21	6.88	1592	9.91	98.3		97.8	
PSA15	3	10.19	6.83	10.24	6.85	1579	8.64	86.0		85.3	
						1510		**91.9**	**8.91**	**91.2**	**8.84**
PSB11	3	12.67	6.65	12.71	6.67	1744	9.73	90.7		90.0	
PSB12	3	12.70	6.78	12.71	6.82	1993	7.90	80.8		79.9	
PSB13	3	12.70	6.81	12.71	6.83	1966	8.51	85.3		84.6	
PSB14	3	12.70	6.81	12.71	6.83	1837	8.61	80.6		80.0	
PSB15	3	12.70	6.81	12.73	6.78	1552	9.47	75.0		75.4	
						1818		**82.5**	**7.10**	**82.0**	**6.78**

seen in Figure 10. This does not imply there is no volume dependency. Rather, because of the unusual amount of scatter, a volume dependency may be obscured.

Figures 9 and 10 show the static strengths for the various specimens from Panel #1 as a function of the nominal cross-sectional area and the ratio of (S/t). Each plot shows a great deal of scatter for a given width or (S/t) ratio. Assuming a volume dependency on the strength, the strength should decrease with increasing cross-sectional area for a given width. This trend is not seen in Figure 10. This does not imply there is no volume dependency. Rather, because of the unusual amount of scatter, a volume dependency may be obscured.

Figure 11 shows the probability distribution of the static transverse tensile strength based on the data from Panel #1. When generating the probability distribution of the strength using Weibull scaling laws, it is best to compare only specimens of similar configurations. However, from a statistical point of view, it is also desirable to have a large number of specimens to evaluate. As each specimen failed in the same mode - transverse tensile failure, it is reasonable, albeit not optimal, to evaluate all of the specimens (n = 59) from Panel #1 as one data set. Using a linear regression technique, the Weibull parameters were found to be m = 5.32 and σ_c = 66.9 Mpa (9.71 ksi). When considering the specimens with a S/t ratio of 3 (n = 22) and 4 (n = 29) individually, the Weibull parameters were found to be m = 5.00, σ_c = 65.7 Mpa (9.53 ksi) and m = 4.90, σ_c = 69.1 Mpa (9.90 ksi) respectively. The results of the static transverse tension strengths are comparable with those found by other investigators for a similar material system tested under three-point bending but with thinner laminates and larger (S/t) ratios; O'Brien and Salkepar, evaluating 33 AS4/3501-6 specimens found m and σ_c to be 7.63 and 61.1 Mpa (8.87 ksi) respectively [5]. The larger m value associated with our data is consistent with the greater scatter of the data. A plot of the probability distribution for the 10 specimens from Panel #2 is

shown in Figure 12 along with the Weibull parameters. The values of m and σ_c were found to be to be 13.0 and 92.2 Mpa (13.38 ksi) respectively.

Transverse Tensile Fatigue Strength Measurements

The results of the fatigue testing can be seen in Figure 13. Individual specimen data (fatigue loading) are found in Table 6. Forty eight different specimens were tested under the conditions of 20 Hz, R = 0.1. At a frequency of 5 Hz, six and five specimens were tested at R = 0.1 and R = 0.5 values respectively. Many tests were stopped at 10^5 and 10^6 cycles. The number in parentheses represents the number of specimens tested at ω = 20 Hz, R = 0.1 that were stopped at 10^5 or 10^6 cycles. The number of tests stopped at 10^5 or 10^6 cycles as well as a fuller description of the testing parameters are given for those specimens that were tested at conditions other than ω = 20 Hz, R = 0.1.

Figure 14 shows four typical specimen failures along with the number of cycles-to-failure for the particular specimens. The specimens all exhibited transverse tensile failures on the lower surface. The final fracture surface exhibited a variety of patterns with the crack "kicking" left or right from the initial failure site. Regardless of whether the final fracture pattern through the thickness of the specimen was nearly vertical or angled, the moment arm l was measured as the distance from the centerline of the edge support roller to the location of tensile failure along the bottom surface of the specimen. The distance δ represents the distance from the centerline of the center loading roller to the location of tensile failure as measured along the bottom surface of the specimen.

TABLE 6--Individual Specimen Data for Transverse Tension Fatigue, 90° Bend Tests.

Specimen ID#	Frequency ω, (Hz)	R	Load Ratio	(S/t)	Nominal Width, w (mm)	Local Width, w (mm)	Thickness, t (mm)	Span, S (mm)	Failure Location δ (mm)	Cycles-to-Failure, Nf	
FA12	20	0.1	0.95	3	10.16	10.21	6.81	20.42	1.49	1420	
FA16	20	0.1	0.95	3	10.16	10.21	6.76	20.27	0.88	210	
FA20	20	0.1	0.95	3	10.16	10.21	6.88	20.65	...	1000000	*
FA23	20	0.1	0.95	3	10.16	10.19	6.78	20.35	...	1000000	*
FA27	20	0.1	0.95	3	10.16	10.21	6.93	20.80	...	100000	*
FA28	20	0.1	0.95	3	10.16	10.19	6.91	20.73	0.60	7920	
FA31	20	0.1	0.95	3	10.16	10.17	6.81	20.42	...	100000	*
FA38	20	0.1	0.95	3	10.16	10.19	6.93	20.80	0.94	1797	
FA47	20	0.1	0.95	3	10.16	10.20	6.90	20.70	12.74	100000	*
FA52	20	0.1	0.95	3	10.16	10.19	6.78	20.35	1.28	34	
FA62	20	0.1	0.95	3	10.16	10.26	6.83	20.50	0.54	2417	
FA63	20	0.1	0.95	3	10.16	10.24	6.81	20.42	0.67	306	
FA11	20	0.1	0.85	3	10.16	10.24	6.83	20.50	0.71	1630	
FA13	20	0.1	0.85	3	10.16	10.29	6.83	20.50	...	1000000	*
FA17	20	0.1	0.85	3	10.16	10.21	6.90	20.69	0.71	720	
FA24	20	0.1	0.85	3	10.16	10.17	6.55	19.66	...	1000000	*
FA26	20	0.1	0.85	3	10.16	10.21	6.78	20.35	...	1000000	*
FA29	20	0.1	0.85	3	10.16	10.19	6.90	20.69	5.58	28	
FA30	20	0.1	0.85	3	10.16	10.19	6.86	20.57	...	1000000	*
FA32	20	0.1	0.85	3	10.16	10.21	6.85	20.54	1.55	352	
FA33	20	0.1	0.85	3	10.16	10.19	6.81	20.42	0.77	310	
FA66	20	0.1	0.85	3	12.70	12.75	6.76	20.27	1.26	3484	
FA68	20	0.1	0.85	3	12.70	12.75	6.92	20.76	0.14	696	
FA70	20	0.1	0.85	3	12.70	12.78	6.86	20.57	...	100000	*
FA72	20	0.1	0.85	3	12.70	12.76	6.78	20.35	0.63	643	
FA74	20	0.1	0.85	3	12.70	12.75	6.91	20.73	0.00	100000	*
FA4	20	0.1	0.80	3	10.16	10.24	6.86	20.57	2.58	130000	
FA6	20	0.1	0.80	3	10.16	10.24	6.74	20.23	0.11	5150	
FA9	20	0.1	0.80	3	10.16	10.20	6.88	20.65	4.74	202100	
FA19	20	0.1	0.80	3	10.16	10.19	6.91	20.73	1.82	73	
FA22	20	0.1	0.80	3	10.16	10.21	6.83	20.50	0.65	100000	*
FA36	20	0.1	0.80	3	10.16	10.21	6.79	20.38	...	100000	*
FA43	20	0.1	0.80	3	10.16	10.19	6.85	20.54	0.86	3675	
FA50	20	0.1	0.80	3	10.16	10.21	6.82	20.46	2.36	361	
FA3	20	0.1	0.75	3	10.16	10.21	6.73	20.19	...	1000000	*
FA8	20	0.1	0.75	3	10.16	10.17	6.90	20.69	...	1000000	*
FA18	20	0.1	0.75	3	10.16	10.17	6.91	20.73	...	100000	*
FA21	20	0.1	0.75	3	10.16	10.19	6.83	20.50	...	100000	*
FA37	20	0.1	0.75	3	10.16	10.20	6.93	20.80	0.33	81089	
FA42	20	0.1	0.75	3	10.16	10.17	6.82	20.46	0.74	65	
FA48	20	0.1	0.75	3	10.16	10.19	6.91	20.73	...	100000	*
FA51	20	0.1	0.75	3	10.16	10.20	6.78	20.35	...	100000	*
FA1	5	0.1	0.85	3	10.16	10.21	6.83	20.50	0.04	6470	
FA2	5	0.1	0.85	3	10.16	10.22	6.81	20.42	1.63	210	
FA39	5	0.1	0.85	3	10.16	10.21	6.93	20.80	1.05	332	
FA41	5	0.1	0.85	3	10.16	10.21	6.85	20.54	3.35	32	
FA46	5	0.1	0.85	3	10.16	10.22	6.78	20.35	...	100000	*
FA53	5	0.1	0.85	3	10.16	10.22	6.86	20.57	0.43	11	
FA40	5	0.5	0.75	3	10.16	10.17	6.83	20.50	...	100000	*
FA49	5	0.5	0.75	3	10.16	10.24	6.91	20.73	0.48	4682	
FA56	5	0.5	0.85	3	10.16	10.24	6.81	20.42	1.49	68877	
FA60	5	0.5	0.85	3	10.16	10.25	6.90	20.69	0.24	8	
FA64	5	0.5	0.85	3	10.16	10.24	6.91	20.73	...	100000	*

Note: * indicates test was stopped at 10^5 or 10^6 cycles.

Failure Location Influence on Strength

The transverse tensile failure location of over 80% of the specimens was within 20% of the distance from the centerline of the center loading roller to the centerline of the support rollers. Figure 15 shows the distribution of the normalized failure location where the normalized failure location is defined as the distance from the center loading roller to the tensile failure location (δ) divided by half the span length ($0.5S$). Two specimens, including FA29 (N=28 cycles) failed under the support roller. In Figure 16, the cycles-to-failure are shown for the various strength ratios as a function of the normalized failure location.

DISCUSSION

Testing of the optimum-sized configuration consistently yielded transverse tensile failures yet still exhibited a great deal of scatter. It was anticipated the smallest configuration would yield transverse tensile failures as from a "Strength of Materials" approach, the ratio of transverse tensile stress to shear stress for a rectangular cross-section subjected to three-point bending is twice the span-to-thickness ratio [*4*]. Considering the transverse tensile strength of 90° graphite/epoxy laminates is of similar magnitude as the shear strength ($\sigma_{TT} \sim 51.7$ MPa, $\tau_{12} \sim 93$ MPa) and considerably smaller than the transverse compressive strength ($\sigma_{TC} \sim 206$ MPa), it would be reasonable to expect failure to initiate at the tensile surface [*7*]. Further, the finite element analysis of the smallest configuration under three-point bending loaded with the average experimental failure load showed the maximum transverse tensile stress was comparable to the transverse tensile strength. It is unclear then whether the large scatter in the static strengths is due to material variability, i.e. inherent presence of flaws or voids, or manufacturing variability, i.e. improper or poor processing of the panels themselves. Considering other researchers have found considerably less scatter when testing 90^0 laminates of comparable material systems in three point bending [*4,5*], it is probable the scatter is due to the manufacturing variability of the particular panels from which the specimens were taken. There did not appear to be a correlation between the failure loads and the number of pits present in a particular specimen. Considering the degree of scatter of transverse strengths in the specimens from Panel #1, it was decided that fatigue specimens would be taken only from Panel #2, whose specimens exhibited considerably less scatter those of Panel #1 under static loading.

Before starting the fatigue testing, certain trends were considered likely to occur. First, a steep S-N curve was considered possible. Although a high moduli graphite/epoxy material

system was being tested, the fibers were oriented in the 90^0 orientation, rather than a 0^0 orientation. Therefore, the matrix would likely see more strain. As the tested laminates are composed solely of 90^0 plies without the benefit of any 'constraining' plies to constrain matrix cracking, once the crack growth reached a Characteristic Damage stage, defined by stable crack growth, damage would progress quickly to failure [*8*]. Recognizing that fatigue strain limit decreases with an increase of off-axis angled plies, opening displacement mode would probably be more important than a sliding displacement occurring parallel to the fibers. Another expectation of the testing was that some specimens would fail by transverse shear failures due to the small (S/t) ratio. Shorter lives were also anticipated due to the testing occurring in load control; displacement and energy control loading have been shown to tend to produce longer lives [*9*].

The original fatigue testing was to be performed at 5 Hz and 0.1 Hz and tests stopped if specimens did not fail after 10^6 cycles. However, initial testing at 5 Hz produced fatigue lives of 10^6 cycles, even at high load ratios. The test program was then modified so tests were performed primarily at 5 Hz and stopped at 10^5 cycles. Examining the S-N curve in Figure 8, it can be seen that the testing produced a great deal of scatter. The number of tests stopped at 10^5 and 10^6 cycles is given in parentheses. Looking only at the highest load ratio, the fatigue lives range from an order of 10^1 to 10^6 cycles. A similar trend can be seen at the other load levels. The range of scatter seems to decrease slightly when looking at the lower load levels. Comparing the data at (P/P_{ult}) equals 0.95 and 0.75, one can see the fatigue lives at the lower load level are generally longer than at the higher load level. Comparing the data for R=0.1 at 20 Hz and 5 Hz, there seems to be little frequency dependency. However, any dependency may be obscured by the large amount of overall scatter of the data. Comparing the fatigue data associated with a

frequency of 5 Hz and R = 0.1 and R = 0.5 values, again, there seems to be little distinction between the two loadings. However, it would be unwise to draw any strong conclusions from this data, as once again there is too much scatter evident.

By taking specimens solely from Panel #2, it was hoped that scatter due to manufacturing, as seen in Panel #1's static strength data, would be minimized. However, if the static results of the specimens from Panel #2 were skewed due to that particular portion of the panel being of very good quality compared to the rest of Panel #2, then the fatigue lives could exhibit substantial scatter. However, this does not seem very likely as the specimens were cut from the portion of the panel with the most uniform C-scan patterns. Other possible sources of scatter could be the lack of edge polishing of the specimens. However, this was purposely not performed so as to mimic 'real-world' structures, which would likely not have their edges polished. Overall, this preliminary study shows that further tests should be performed in order to determine whether the variability of the data was due primarily to panel and/or specimen preparation or due to material variability, inherent in the 90^0 bend specimen.

CONCLUSIONS

Researchers have found in bonded skin/stiffener/frame composite reinforced panels, failure initiated in adhesive pocket at the interface of the skin/stiffener and propagated as transverse crack in skin laminate or flange laminate near the flange tip. A finite element analysis was performed to evaluate the validity of the result, based on a "Strength of Materials" approach, that the ratio of the maximum transverse tensile stress to maximum shear stress equals twice the span-to-thickness (*S/t*) ratio. Modelling a small three-point bend specimen, corresponding to a specimen with width = 10.2 mm, t = 6.76 mm, (*S*/t) = 3, a nonlinear static finite element analysis was performed. The finite element model produced a ratio of the predicted maximum transverse tensile stress to predicted maximum shear stress of 5.28 whereas the "strength of materials" approach for the same sized configuration would predict a ratio of 6. The predicted maximum longitudinal tensile stress was comparable to the transverse tensile strength. However, the maximum longitudinal compressive stress, located just under the central roller, was also comparable to the transverse compression strength. Further discretization of the existing finite element model near the central roller contact point should be performed.

An experimental investigation of the transverse tensile strength of IM6/3501 composite materials was then performed on specimens subjected to three-point bending under static and fatigue loading. In this study, a parametric study of (S/t) effects was performed experimentally to determine an "optimum" configuration where optimum was defined as the smallest configuration which consistently failed in transverse tension when subjected to three-point bending under static loading. The optimum configuration was found to be specimens with nominal dimensions of (S/t) equal 3 and width equal 10.2 mm (0.4 inches). Fatigue testing under three-point bending was performed on specimens of the optimum configuration. The S-N data

showed a great deal of scatter. At this time, it is unclear whether the scatter in the data is due primarily to material variability (i.e. the presence of voids or flaws) or manufacturing variability (i.e. improper preparation of panels and/or specimens).

Future work should begin with tension fatigue testing under similar test conditions of 90 degree laminates taken from Panel #2. This would provide insight into the integrity of the three-point bend test procedure. Additional fatigue testing should also include testing under three-point bending of similar-sized specimens as the transverse bending specimens used in this study taken from panels manufactured by different sources. These tests would be performed at similar conditions as the current study. Testing of thinner laminates performed under similar conditions should also be undertaken to monitor to assess sizing effects due to thickness of the laminate and clumping of same-angle plies. Periodic monitoring of the edges and crack growth would be beneficial in further understanding of the fatigue growth. A comparison of these results may provide understanding into whether the scatter observed in this study is due to material variability or manufacturing variability. If the data produced less scatter, fatigue growth laws could possibly be determined.

ACKNOWLEDGMENTS

This work was initiated as a result of the NASA-ASEE Summer Faculty Fellowship program. This work was funded in part by NASA Langley Research Center through grant NAG-1-1773. Special thanks go to Drs. T.K. O'Brien of the Mechanics of Materials Branch, NASA LaRC and P.J. Minguet of the Boeing Defense & Space Group, Helicopters Division, Philadelphia, PA as well as S. and R. Coguill of the Composites Materials Research Group (CMRG) of the University of Wyoming, Laramie, WY.

REFERENCES

[1] Minguet, P.J., Fedro, M., O'Brien, T.K., Martin, R., Ilcewicz, L., Awerbuch, J., and Wang, A., "Development of a Structural Test Simulating Pressure Pillowing Effects in a Bonded Skin/Stringer/Frame Configuration," Presented at Fourth NASA/DoD Advanced Composite Technology (ACT) Conference, NASA-CP 3229, Salt Lake City, UT, 1993, pp. 863-880.

[2] Minguet, P.J. and O'Brien, T.K., "Analysis of Composite Skin/Stringer Bond Failure Using a Strain Energy Release Rate Approach," Presented at 1995 ICCM Conference, Vancouver, August 1995.

[3] *Fatigue of Composite Materials,* K.L. Reifsnider, Ed., Elsevier Science Publishers B.V., 1990, pp. 105–158.

[4] Adams, D.F., King, T.R., and Blackketter, D.M., "Evaluation of the Transverse Flexure Test Method for Composite Materials," *Composite Science and Technology,* Elsevier Science Publishers, Ltd., England, 1990, pp. 341-353.

[5] O'Brien, T.K. and Salpekar, S.A., "Scale Effects on the Transverse Tensile Strength of Graphite/Epoxy Composites," *Composite Materials: Testing and Design (Eleventh Volume),* ASTM STP 1206, E.T. Camponeschi, Jr.,Ed., American Society for Testing and Materials, Philadelphia, PA 1993, pp. 23-42.

[6] Weibull, W., "A Statistical Theory of the Strength of Materials," Ing. Vetenskaps Akad. Handl. *(Royal Swedish Institute Engineering Research Proceedings),* NR151, 1939.

[7] Tsai, S.W. and Hahn, H.T., *Introduction to Composite Materials,* Technomic Publishing Company, Lancaster, PA, 1980, pp. 293-294.

[8] Reifsnider, K.L., Henneke, E.G., Stinchcomb, W.W., and Duke, J.C., in "*Mechanics of Composite Materials, Recent Advances,*" Z. Hashin and C.T. Herakovich, Eds., Pergamon Press, New York, 1983, pp. 399-420.

[9] *Fatigue of Composite Materials,* K.L. Reifsnider, Ed., Elsevier Science Publishers B.V., 1990, pp. 158-161

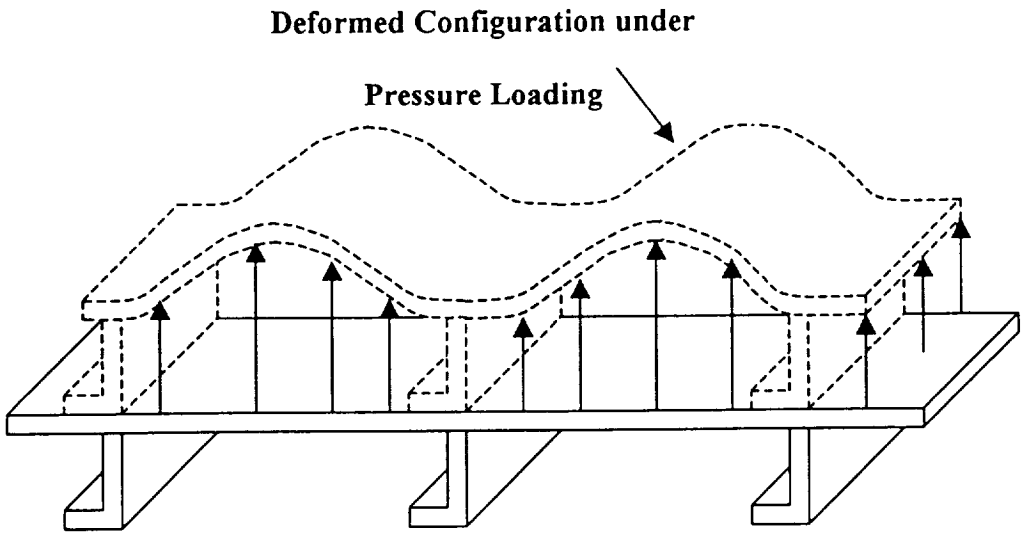

Figure 1. Illustration of Pressure Pillowing in a Pressurized Fuselage

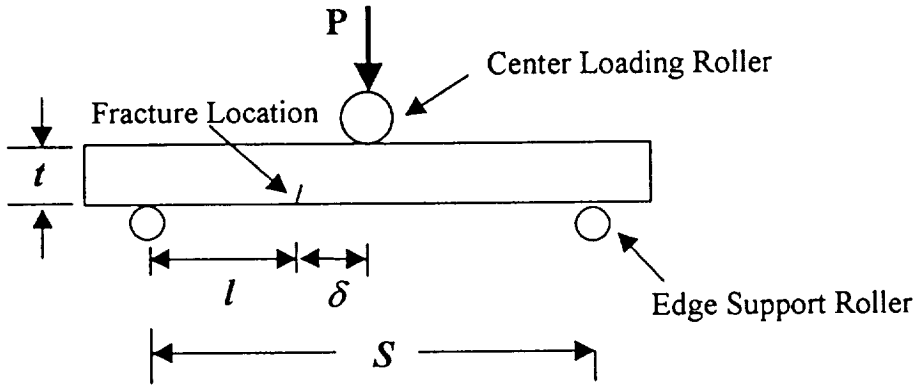

Figure 2. Schematic of Test Set-up

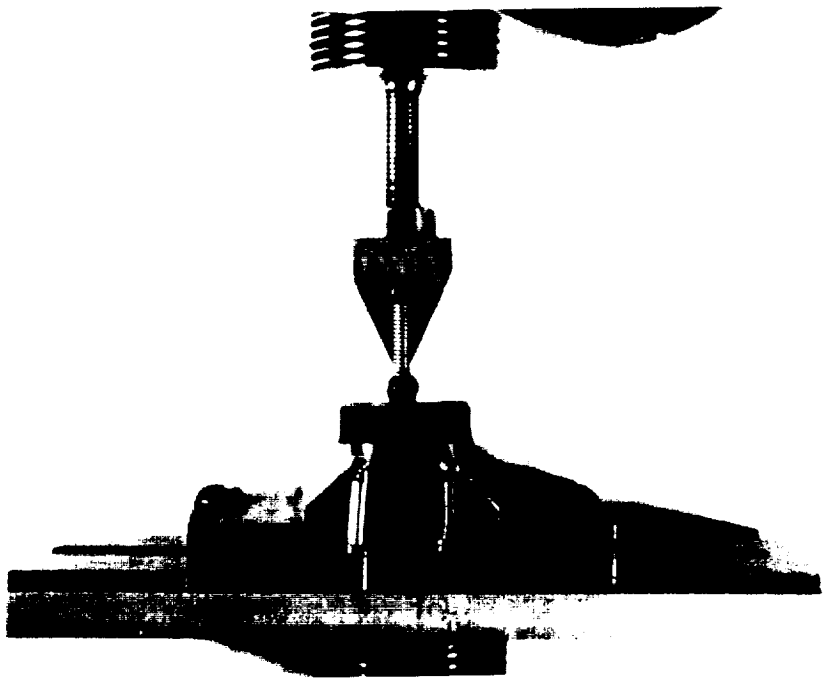

Figure 3. Three-Point Bend Test Set-up

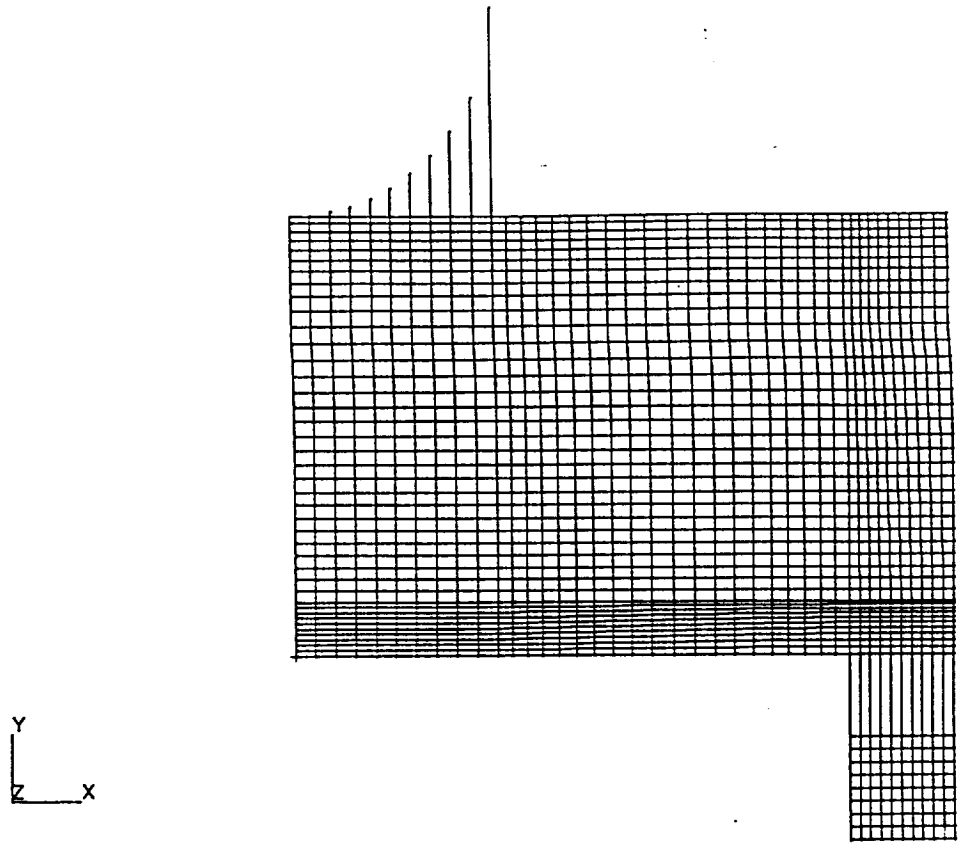

Figure 4. Finite Element Mesh

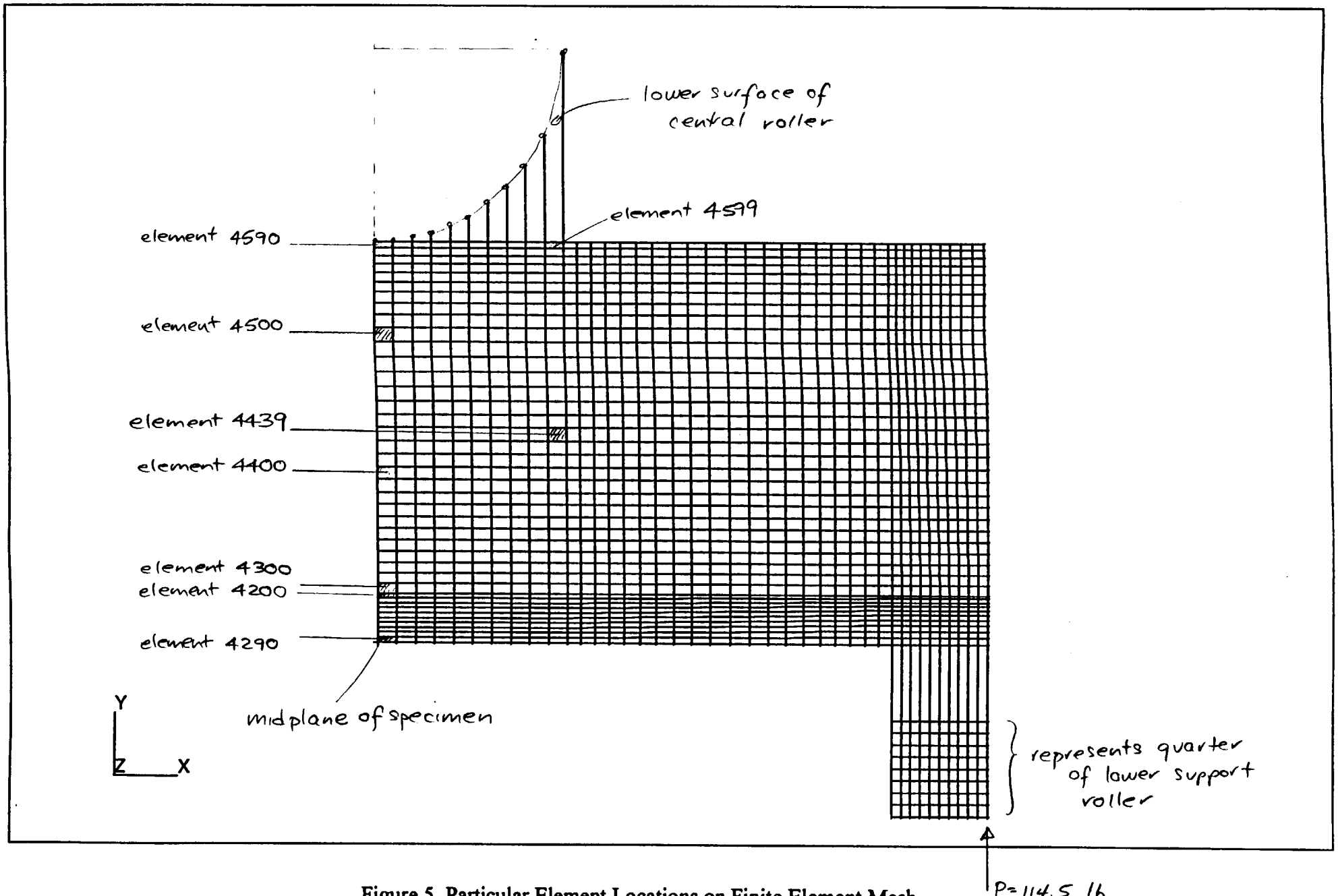

Figure 5. Particular Element Locations on Finite Element Mesh

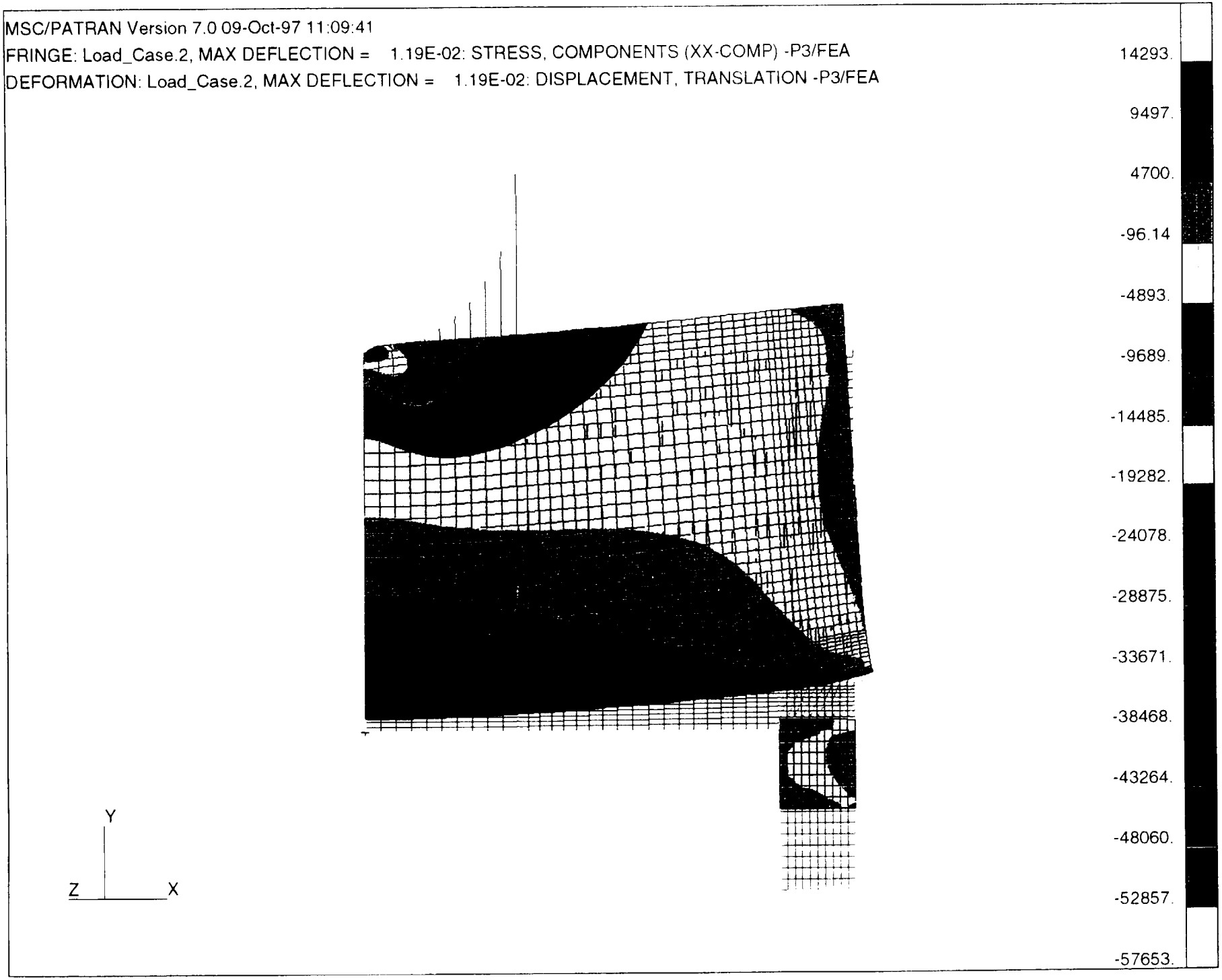

Figure 6 Global Longitudinal Stresses(σ_x) from Finite Element Mesh

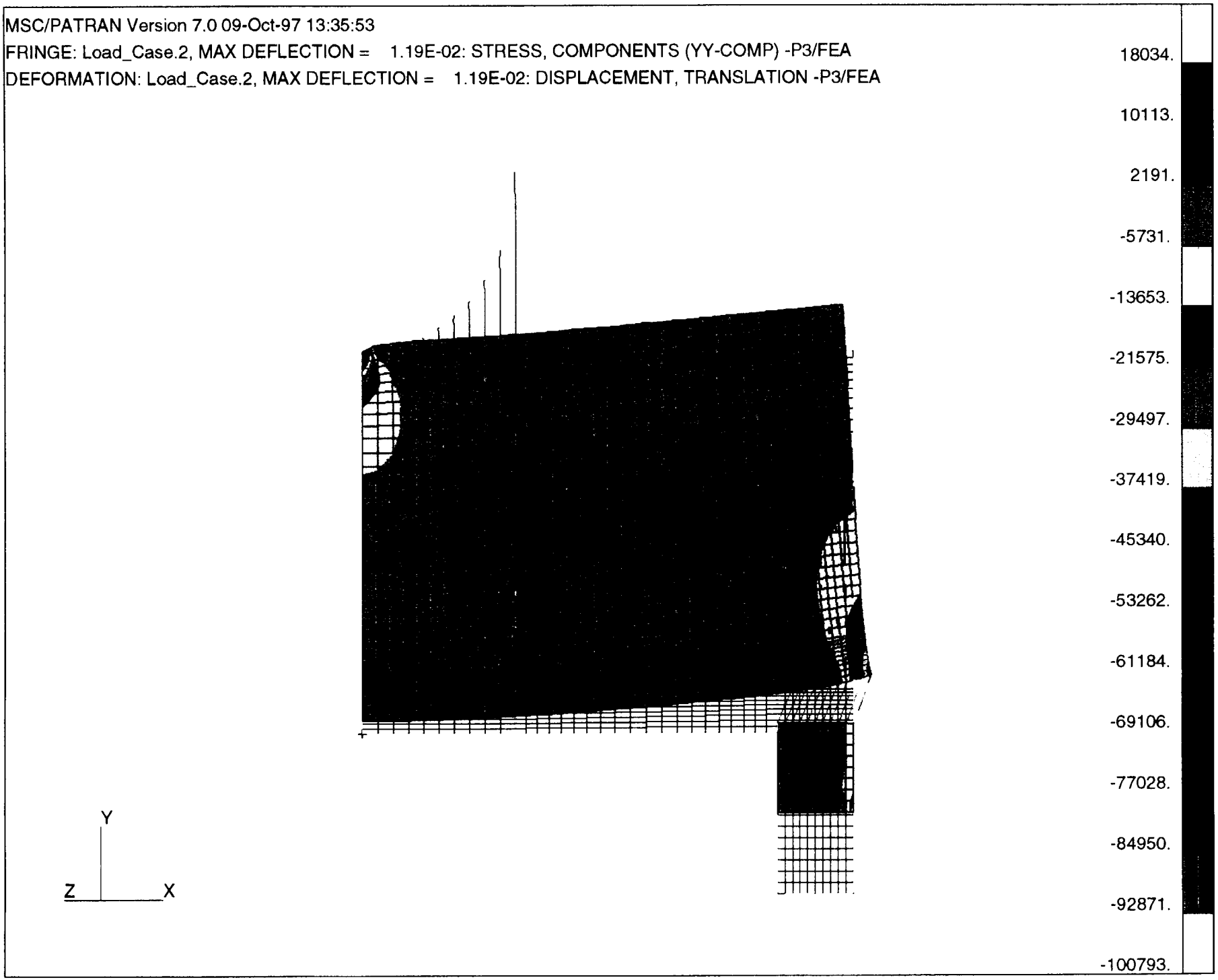

Figure 7. Global Transverse Stresses (σ_y) from Finite Element Mesh

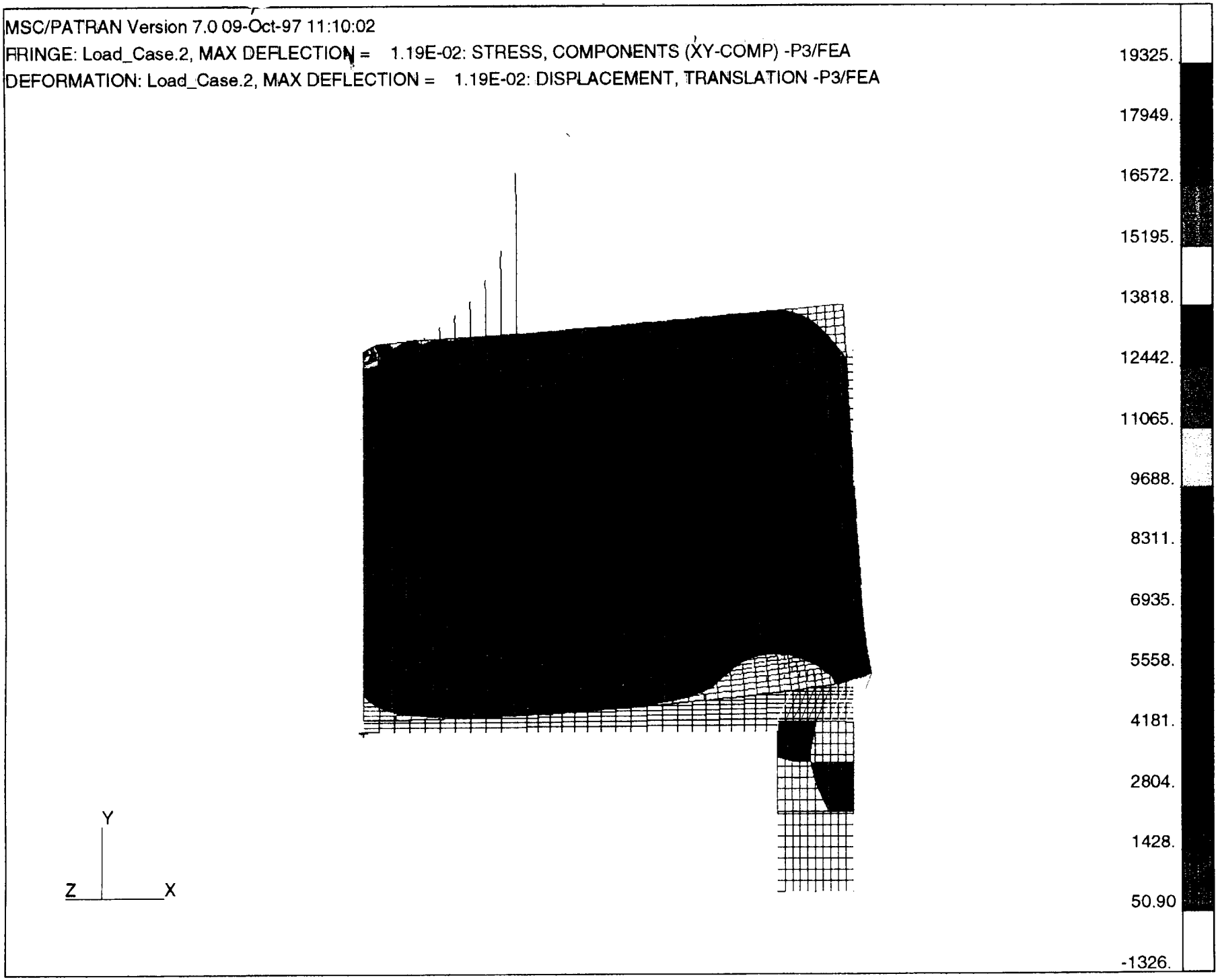

Figure 8. Global Shear Stresses (τ_{xy}) from Finite Element Mesh

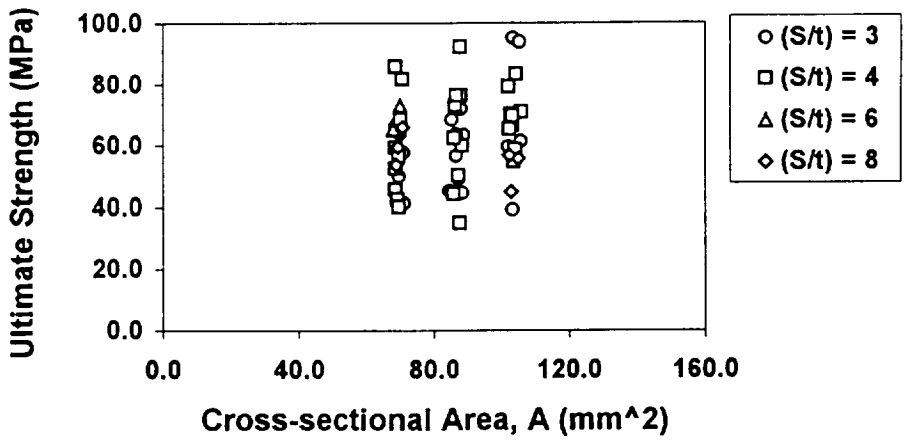

Figure 9. Effect of Nominal Cross-sectional Area on Transverse Tensile Strength, Panel #1

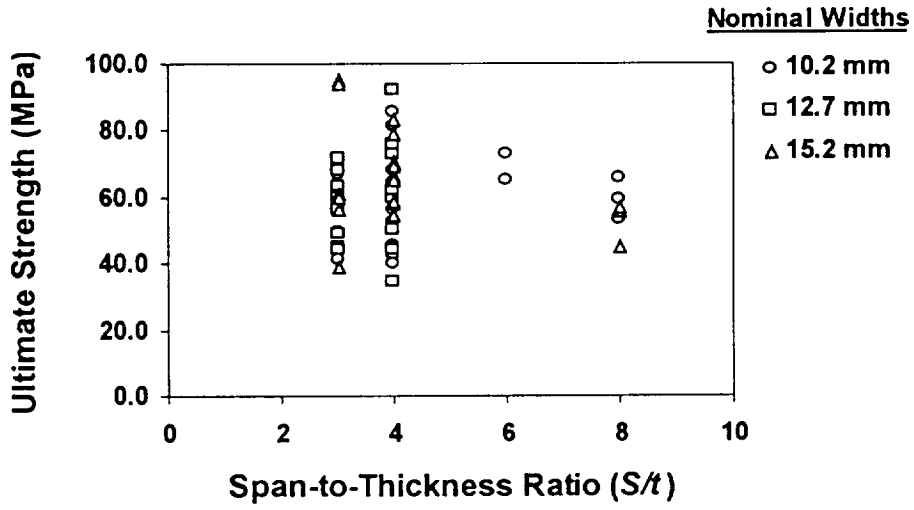

Figure 10. Effect of (S/t) Ratio on Transverse Tensile Strength, Panel #1

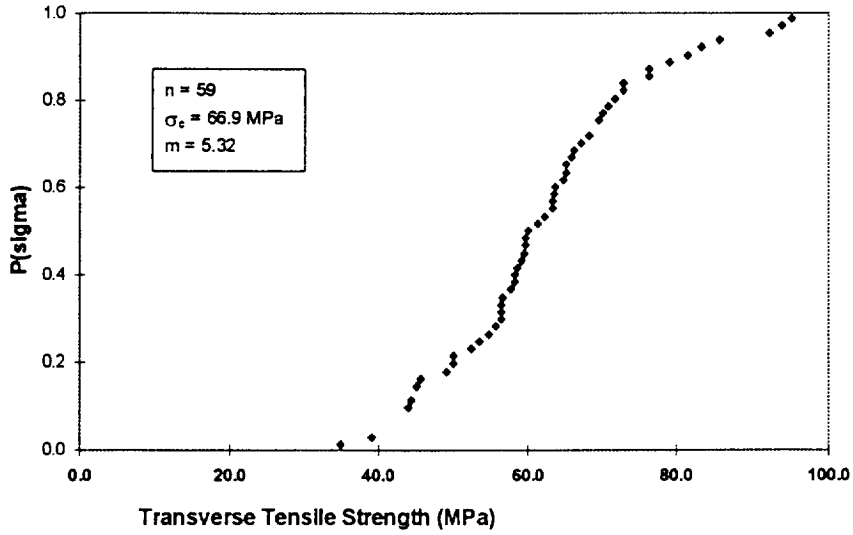

Figure 11. Probability Distribution of the Static Transverse Tensile Strength, Panel #1

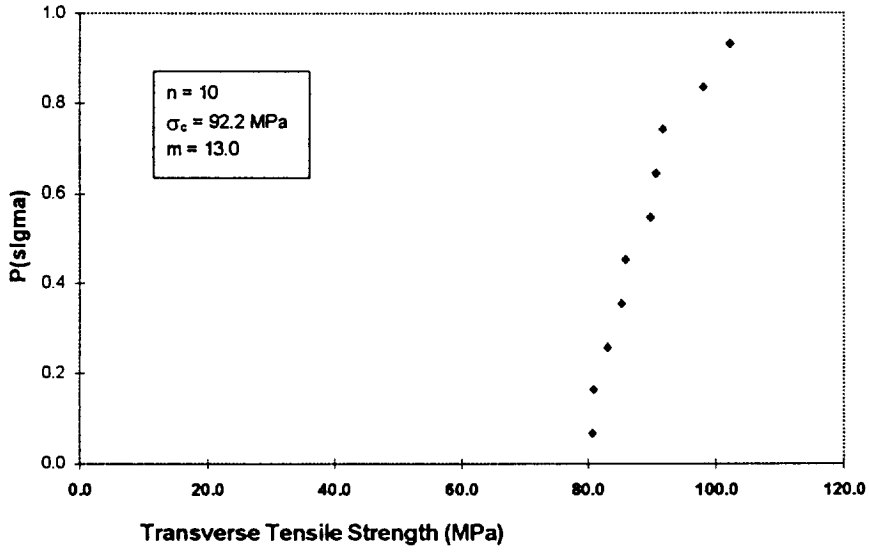

Figure 12. Probability Distribution of the Static Transverse Tensile Strength, Panel #2

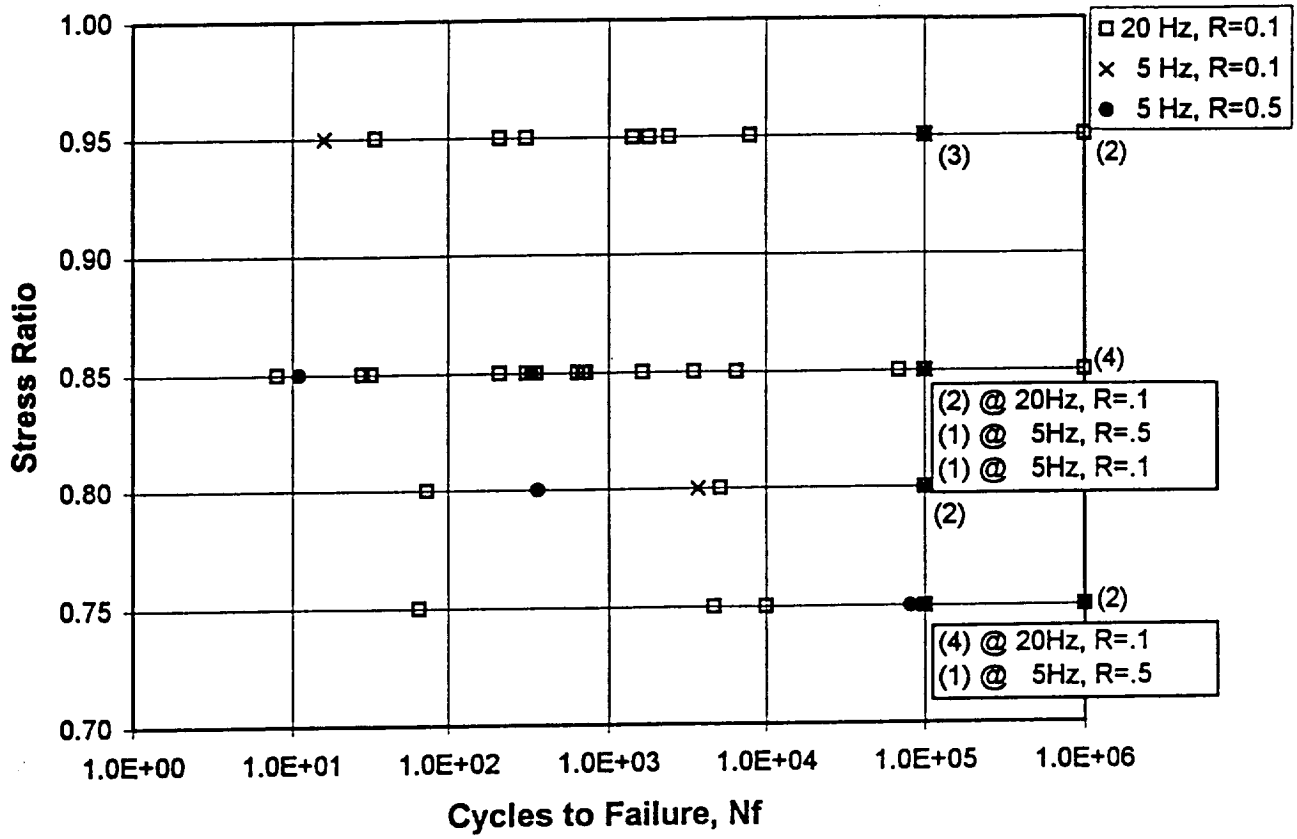

Figure 13. Transverse Tension S-N Curve under Three-Point Bending (Number of tests stopped at 10^5 and 10^6 cycles given in parentheses)

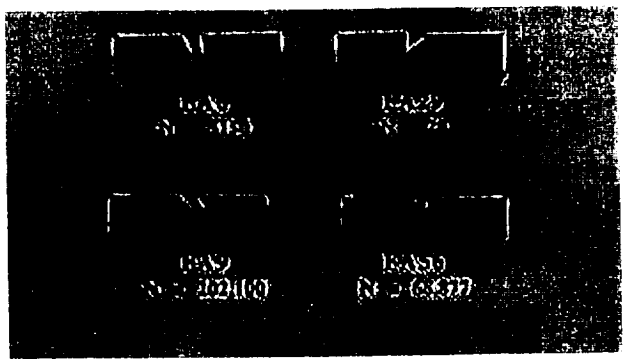

Figure 14. Representative Transverse Tension Fatigue Failures

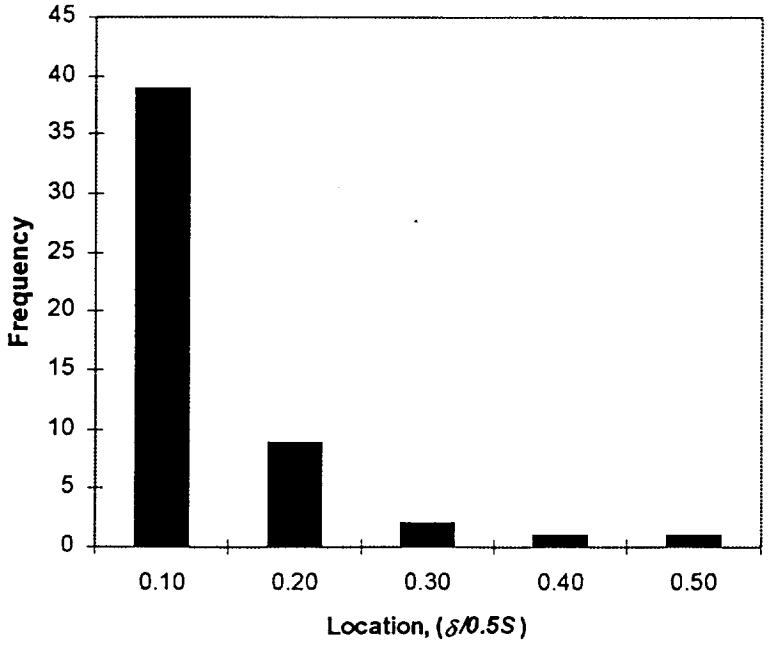

Figure 15. Distribution of the Normalized Failure Location of Transverse Tension Fatigue Data

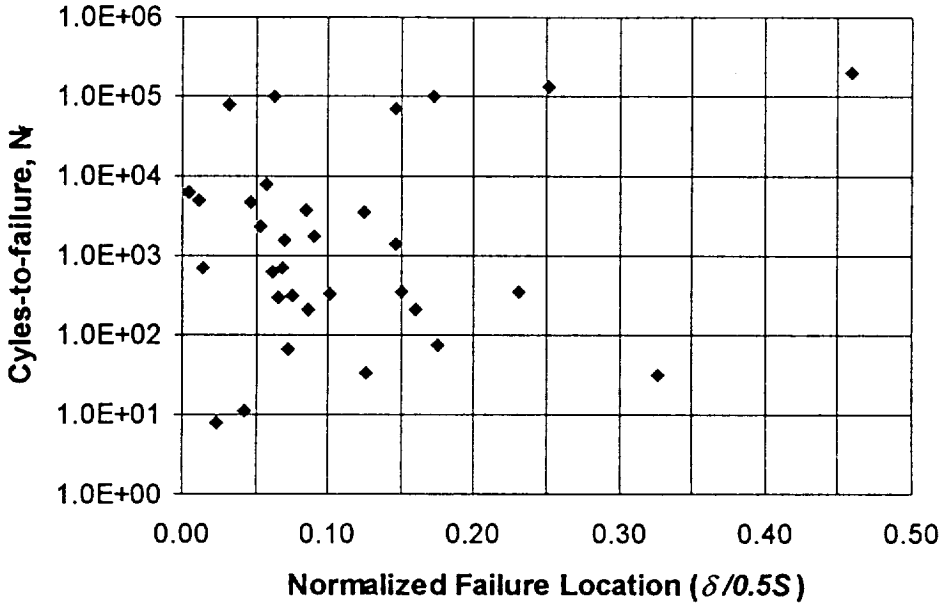

Figure 16. Effect of the Normalized Failure Location on Transverse Tension Fatigue Cycles-to-Failure